

NUMERICAL EXPERIMENTS ON THE PERFECT MATCHING OF PERFECTLY MATCHED LAYERS

DANIEL APPELÖ AND THOMAS HAGSTROM

1. INTRODUCTION

In this brief note we describe numerical experiments designed to examine the perfect matching property of the perfectly matched layers (PML) described in [AHK06] and [CT01]. To contrast the results obtained with PML we perform simulations with a simple absorbing layer with an “unmatched” lower order damping term. The numerical method (detailed below) we use discretizes the interior computational domain and the layer separately. Coupling of the domains are enforced by equating characteristic information at the interface. The error of caused by the coupling is assessed in a separate computation, where a layer, without damping (i.e. we solve Maxwell’s equations everywhere), is coupled to the interior computational domain.

2. MODAL PML

We consider the scaled TM_z problem in a lossless medium.

$$(1) \quad \begin{aligned} \frac{\partial E^z}{\partial t} - \frac{\partial H^y}{\partial x} + \frac{\partial H^x}{\partial y} &= 0, \\ \frac{\partial H^x}{\partial t} + \frac{\partial E^z}{\partial y} &= 0, \\ \frac{\partial H^y}{\partial t} - \frac{\partial E^z}{\partial x} &= 0, \end{aligned}$$

and the corresponding PML

$$(2) \quad \begin{aligned} \frac{\partial E^z}{\partial t} - \eta \left(\frac{\partial H^y}{\partial x} + \sigma \phi^{(1)} \right) + \frac{\partial H^x}{\partial y} &= 0, \\ \frac{\partial H^x}{\partial t} + \frac{\partial E^z}{\partial y} &= 0, \\ \frac{\partial H^y}{\partial t} - \eta \left(\frac{\partial E^z}{\partial x} + \sigma \phi^{(2)} \right) &= 0, \\ \frac{\partial \phi^{(1)}}{\partial t} + \frac{\partial E^z}{\partial x} + (\sigma + \alpha) \phi^{(1)} &= 0, \\ \frac{\partial \phi^{(2)}}{\partial t} + \frac{\partial H^y}{\partial x} + (\sigma + \alpha) \phi^{(2)} &= 0. \end{aligned}$$

Here σ is the damping, α the complex frequency shift [Pet00] and η is a strictly positive function corresponding to grid stretching inside the PML.

2.1. A Numerical experiment. In this experiment, described in Figure 1, we place initial data

$$E^z(x, y) = Ae^{-\sigma^2((x-x_s)^2+(y-y_s)^2)}, \quad H^x(x, y) = 0, \quad H^y(x, y) = 0,$$

with $A = 1$, $(x, y) = (1.5, 0.5)$, inside the y -periodic rectangle $(x, y) \in \Omega_R = [-2, 2] \times [0, 1]$. The solution to this problem is symmetric about $x = 1.5$ so we can measure the reflection from the PML by comparing the solution along the dashed lines, $x = 1.05$ and $x = 1.95$, see Figure 1. Inside the rectangle Ω_R we solve (1) and inside the layers we solve (2). The parameter η in (2) will be set to 1 everywhere, i.e. no grid stretching is employed.

Date: May 8, 2009.

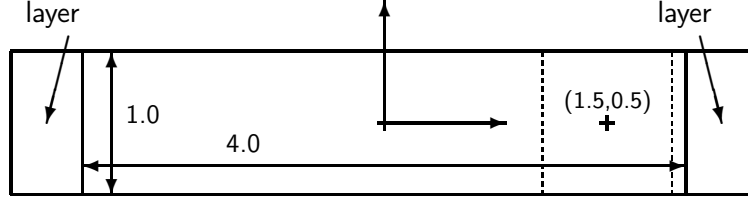


FIGURE 1. Schematic picture of the setup of the first example.

As we are interested in the perfect matching, or non-reflectivity of the PML *interface* we let the PML be sufficiently wide, 3 length units, for the boundary conditions at the end of the PML not to have any influence. We use a constant damping function $\sigma = 10$ and discretize the equations in the layer and in Ω_R separately and couple the solutions by equating the characteristic variables at the interface (we describe the details below). Finally we take the complex frequency shift equal to zero in order to mimic the form of Bérenger's PML [B94] as closely as possible.

2.1.1. *Discretization.* In space we will discretize (1) and (2) using finite difference methods. As we take the damping function to be constant it is not suitable to use difference stencils that cross the interface. Instead we approximate the derivatives w.r.t. x in (1) and (2) by using one-sided approximations close to the interface. Communication between the domains is handled by equating the characteristic variables.

To obtain maximal order of accuracy of the spatial discretization we use grid-stabilized difference approximations [HH07]. We describe the discretization procedure in detail for the rectangular inner domain, Ω_R . Let Ω_R be partitioned by the union of the equidistant grid

$$\begin{aligned} x_i &= -2 + ih, \quad i = 0, \dots, n = 4m, \\ y_j &= jh, \quad j = 0, \dots, m, \quad h = 1/m, \end{aligned}$$

and the additional points

$$(3) \quad \begin{aligned} x_l &= -2 + h/5, \quad y_{lj} = jh, \quad j = 0, \dots, m, \\ x_r &= 2 - h/5, \quad y_{rj} = jh, \quad j = 0, \dots, m. \end{aligned}$$

In the grid points the fields $E^z(x_i, y_j)$, $H^x(x_i, y_j)$ and $H^y(x_i, y_j)$ are approximated by the grid functions E_{ij}^z , H_{ij}^x and H_{ij}^y . Away from the boundaries we approximate derivatives using the eight-order-accurate stencil

$$(4) \quad \frac{\partial u(x_i, y_j, t)}{\partial x} \approx D_0^x \left(1 - \frac{h^2}{6} D_+^x D_-^x + \frac{h^4}{30} (D_+^x D_-^x)^2 - \frac{h^6}{140} (D_+^x D_-^x)^3 \right) u_{ij}(t),$$

where

$$D_0^x u_i = \frac{u_{i+1} - u_{i-1}}{2h}, \quad D_+^x u_i = D_-^x u_{i+1} = \frac{u_{i+1} - u_i}{h}.$$

Close to the boundary we follow [HH07] and use the derivative of the 8th-degree-interpolating polynomial constructed from the data at the target node and its 8 closest neighbors. The additional nodes (3) are injected to suppress Runge's phenomena and stabilizes the approximation. Derivatives w.r.t. y are approximated everywhere using the y direction version of (4) and the periodic boundary conditions. The discretizations inside the layers are analogous.

The solution on each subdomain is advanced in time using the classic fourth-order-accurate Runge-Kutta method. After each substep and at the completion of a full step we update the values at the left interface according to the sequence:

1. $r_1 = E_l^z - H_l^y$, $r_3 = E^z + H^y$.
2. $H_l^x = H^x$, $E_l^z = E^z = \frac{r_1 + r_3}{2}$, $H_l^y = H^y = \frac{r_3 - r_1}{2}$.

At the right interface we use:

1. $r_1 = E^z - H^y$, $r_3 = E_r^z + H_r^y$.
2. $H_r^x = H^x$, $E_r^z = E^z = \frac{r_1 + r_3}{2}$, $H_r^y = H^y = \frac{r_3 - r_1}{2}$.

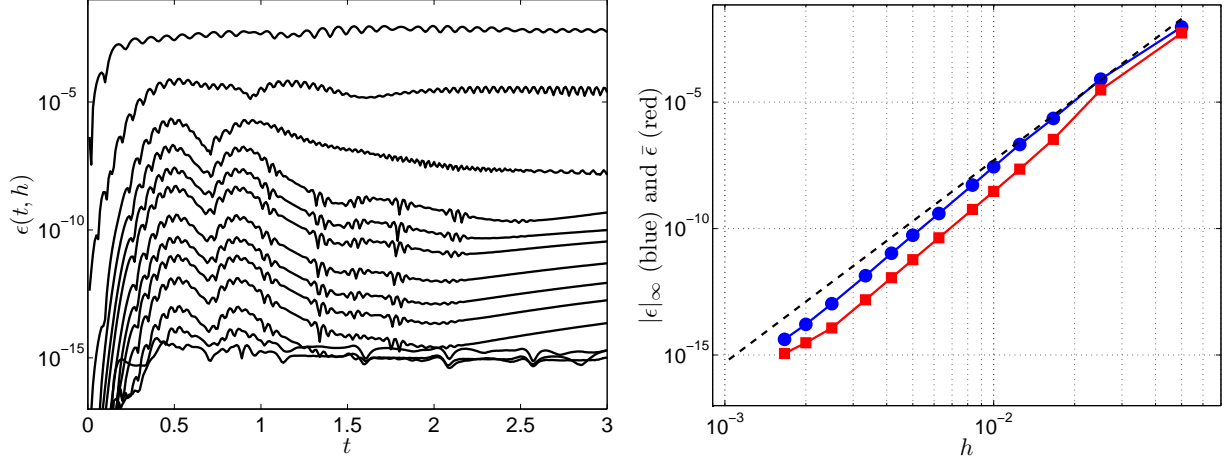


FIGURE 2. Results for the modal PML. To the left the error $\epsilon(t, h)$ is plotted as a function of $h = 1/20r$, with $r = 1, \dots, 6, 8, 10, 12, 15, 20, 25, 30$. To the right, the maximum (blue with circles) and the mean (red with squares) of $\epsilon(t, \cdot)$ are plotted as a function of h . The black dashed line indicates $\sim h^8$.

We measure the reflection by computing the error:

$$(5) \quad \epsilon(t, h) = \left(\sum_{j=1}^m h (E_{i_a j}^z - E_{i_b j}^z)^2 \right)^{\frac{1}{2}}.$$

Here i_a and i_b are the indices such that $x_{i_a} = 1.05$, $x_{i_b} = 1.95$.

2.2. Results. We perform computations using the method described above on grids with $m = 20r$, $r = 1, \dots, 6, 8, 10, 12, 15, 20, 25, 30, 40, 50$. The solution is advanced up to time 3 using a timestep $k = \frac{1}{200r}$.

In Figure 2 we have plotted the maximum and mean of $\epsilon(t, h)$ on the time interval $[0, 3]$ as a function of the grid spacing, h . From the dashed line, which is $\sim h^8$, it can be seen that error is reduced at the rate $\mathcal{O}(h^8)$ until we reach machine precision. To the left in Figure 2 have also plotted the time histories of $\epsilon(t, h)$ for different refinement.

3. BÉRENGER'S PML – COLLINO AND TSOGKA STYLE

The formulation of Bérenger's PML following Collino and Tsogka [CT01] can be written

$$(6) \quad \begin{aligned} \frac{\partial E_1^z}{\partial t} - \frac{\partial(H_1^y + H_2^y)}{\partial x} &= -\sigma E_1^z, \\ \frac{\partial H_1^x}{\partial t} &= -\sigma H_1^x, \\ \frac{\partial H_1^y}{\partial t} - \frac{\partial(E_1^z + E_2^z)}{\partial x} &= -\sigma H_1^y, \\ \frac{\partial E_2^z}{\partial t} + \frac{\partial(H_1^x + H_2^x)}{\partial y} &= 0, \\ \frac{\partial H_2^x}{\partial t} + \frac{\partial(E_1^z + E_2^z)}{\partial y} &= 0, \\ \frac{\partial H_2^y}{\partial t} &= 0. \end{aligned}$$

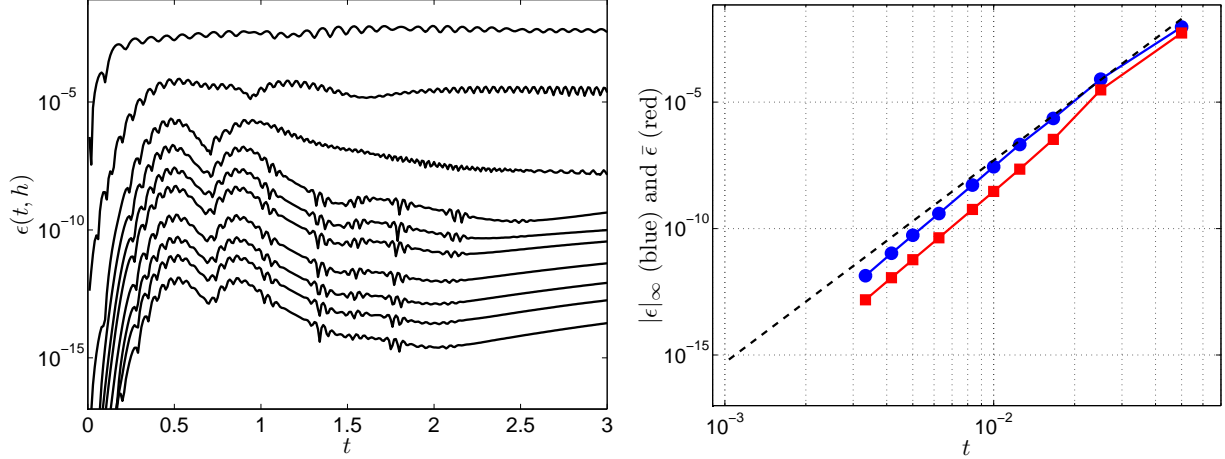


FIGURE 3. Results for Collino and Tsogka's PML. To the left the error $\epsilon(t, h)$ is plotted as a function of $h = 1/20r$, with $r = 1, \dots, 6, 8, 10, 12$. To the right, the maximum (blue with circles) and the mean (red with squares) of $\epsilon(t, \cdot)$ are plotted as a function of h . The black dashed line indicates $\sim h^8$.

The x characteristics of (6) are

$$\begin{aligned} r_1 &= (E_1^z + E_2^z) - (H_1^y + H_2^y), \\ r_2 &= (E_1^z + E_2^z) + (H_1^y + H_2^y), \\ r_3 &= H_2^y, \quad r_4 = H_2^x, \quad r_5 = E_2^z, \quad r_6 = H_1^x. \end{aligned}$$

Here r_1 is right-going and r_2 left-going, the rest are characteristic. Thus at the right interface we must update the boundary conditions according to

- (1) $r_1 = E^z - H^y$, $r_2 = (E_1^z + E_2^z) + (H_1^y + H_2^y)$, $r_3 = H_2^y$, $r_4 = H_2^x$, $r_5 = E_2^z$, $r_6 = H_1^x$,
- (2) $E_1^z = \frac{r_1 + r_2}{2} - r_5$, $H_1^y = \frac{r_2 - r_1}{2} - r_3$,
- (3) $E^z = E_1^z + E_2^z$, $H^x = H_1^x + H_2^x$, $H^y = H_1^y + H_2^y$.

3.1. Simulation results. We redo the experiments described in §2.1 with the discretization detailed in §2.1.1. In Figure 3 we plot time histories and the max and mean of the error $\epsilon(t, h)$. The results are quite similar to those of the modal PML.

4. A SIMPLE NON-MATCHED LAYER

To contrast the results obtained with the above PML we repeat the numerical experiments of §2.1 truncating the domain with the simple damping layer

$$(7) \quad \begin{aligned} \frac{\partial E^z}{\partial t} - \frac{\partial H^y}{\partial x} + \frac{\partial H^x}{\partial y} &= -\sigma E^z, \\ \frac{\partial H^x}{\partial t} + \frac{\partial E^z}{\partial y} &= -\sigma H^x, \\ \frac{\partial H^y}{\partial t} - \frac{\partial E^z}{\partial x} &= -\sigma H^y. \end{aligned}$$

As can be seen in Figure 5 the equations are not matched and there is a reflection caused by the interface that make the error converge to a fixed level.

5. A COMPUTATION WITHOUT DAMPING

To assess the error caused by the coupling via characteristic data at the interface we set $\sigma = 0$ and redo the computations of §2.1 with the exception that the layer width is taken to be 1. Making the layer this

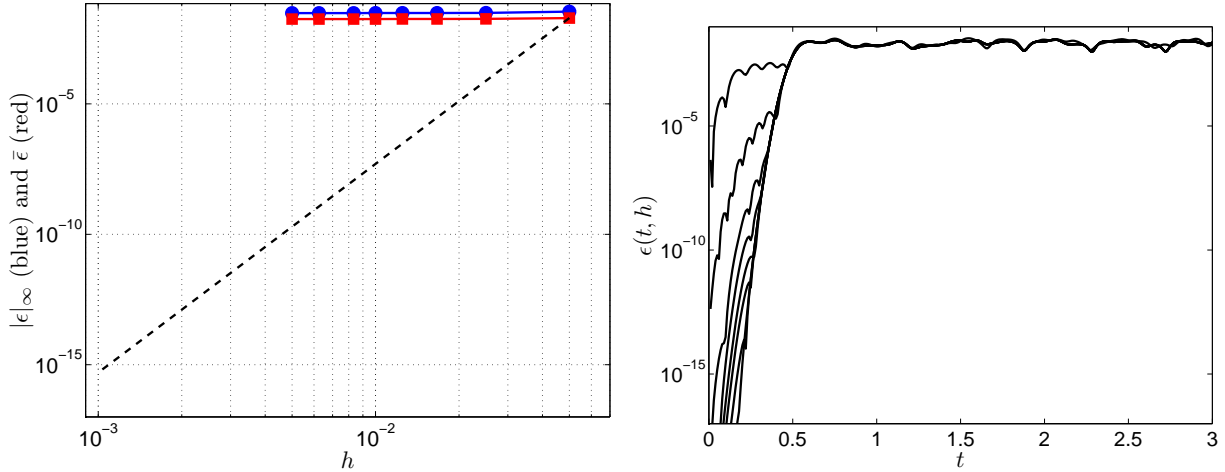


FIGURE 4. Results for the simple layer (7). To the left the error $\epsilon(t, h)$ is plotted as a function of $h = 1/20r$, with $r = 1, \dots, 5$. To the right, the maximum (blue with circles) and the mean (red with squares) of $\epsilon(t, \cdot)$ are plotted as a function of h . The black dashed line indicates $\sim h^8$.

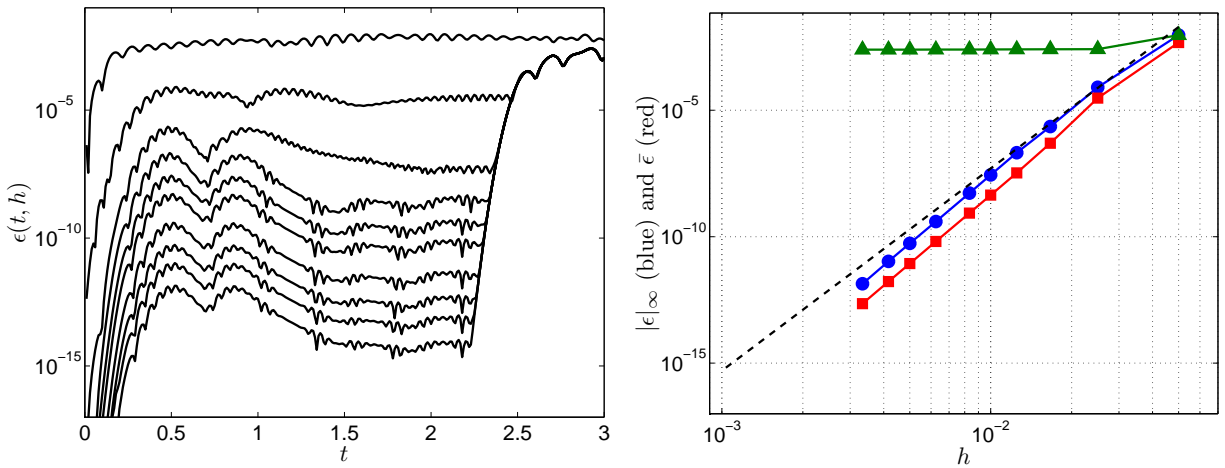


FIGURE 5. Results for a thin layer terminated by characteristic boundary conditions. To the left the error $\epsilon(t, h)$ is plotted as a function of $h = 1/20r$, with $r = 1, \dots, 6$. To the right, the maximum (blue with circles), the mean (red with squares) of $\epsilon(t, \cdot)$, $t \in [0, 2]$ and maximum (green with triangles) of $\epsilon(t, \cdot)$, $t \in [0, 3]$, are plotted as a function of h . The black dashed line indicates $\sim h^8$.

thin allow us also to see the influence of the boundary conditions terminating the PML (extrapolation of the characteristic data).

In Figure 5 it can be seen that the errors (before $t \approx 2$) without the damping are very similar to those computed when the damping is present. This is a strong indication that the layers (2) and (6) are indeed reflection-less, at least for this example. The rapid rise of $\epsilon(t, h)$ around $t = 2$ is caused by the reflections from the extrapolation boundary conditions at the end of the (thin) layer.

REFERENCES

- [AHK06] D. Appelö, T. Hagstrom, and G. Kreiss, *Perfectly matched layers for hyperbolic systems: General formulation, well-posedness, and stability*, SIAM Journal on Applied Mathematics **67** (2006), no. 1, 1–23.

- [B94] J. Bérenger, *A perfectly matched layer for the absorption of electromagnetic waves*, J. Comput. Phys. **114** (1994), 185.
- [CT01] F. Collino and C. Tsogka, *Application of the PML absorbing layer model to the linear elastodynamic problem in anisotropic heterogeneous media*, Geophysics **66** (2001), no. 1, 294–307.
- [HH07] Thomas Hagstrom and George Hagstrom, *Grid stabilization of high-order one-sided differencing I: First-order hyperbolic systems*, Journal of Computational Physics **223** (2007), no. 1, 316–340.
- [Pet00] P.G. Petropoulos, *Reflectionless sponge layers as absorbing boundary conditions for the numerical solution of Maxwell equations in rectangular, cylindrical and spherical coordinates*, SIAM J. Appl. Math. **60** (2000), no. 3, 1037–1058.

APPLIED & COMPUTATIONAL MATHEMATICS, CALIFORNIA INSTITUTE OF TECHNOLOGY, PASADENA, CA 91125
E-mail address: appelo@caltech.edu
URL: www.its.caltech.edu/~appelo

DEPARTMENT OF MATHEMATICS, SOUTHERN METHODIST UNIVERSITY, DALLAS, TX 75275
E-mail address: thagstrom@smu.edu
URL: <http://faculty.smu.edu/thagstrom>